Revisiting Nonlocal Electron-Energy Transport in Inertial-Fusion Conditions

G. Schurtz,[1] S. Gary,[2] S. Hulin,[3] C. Chenais-Popovics,[4] J.-C. Gauthier,[1] F. Thais,[5] J. Breil,[1] F. Durut,[6] J.-L. Feugeas,[1] P.-H. Maire,[1] P. Nicolaï,[1] O. Peyrusse,[1] C. Reverdin,[2] G. Soullié,[2] V. Tikhonchuk,[1] B. Villette,[2] and C. Fourment[1]

[1]*Université Bordeaux 1; CNRS; CEA, Centre Lasers Intenses et Applications, 33405 Talence, France*

[2]*CEA/DIF, 91680 Bruyères-le-Châtel, France*

[3]*CEA/CESTA, 33114 Le Barp, France*

[4]*Laboratoire pour l'Utilisation des Lasers Intenses, UMR 7605, CNRS; CEA; Université Paris VI; Ecole Polytechnique, 91128 Palaiseau, France*

[5]*CEA/DSM, 91191 Gif sur Yvette, France*

[6]*CEA/VA, 21120 Is sur Tille, France*

(Received 9 September 2006; revised manuscript received 4 December 2006; published 27 February 2007)

Correct modeling of the electron-energy transport is essential for inertial confinement fusion target design. Various transport models have been proposed in order to extend the validity of a hydrodynamical description into weakly collisional regimes, taking into account the nonlocality of the electron transport combined with the effects of self-generated magnetic fields. We have carried out new experiments designed to be highly sensitive to the modeling of the heat flow on the Ligne d'Intégration Laser facility, the prototype of the Laser Megajoule. We show that two-dimensional hydrodynamic simulations correctly reproduce the experimental results only if they include both the nonlocal transport and magnetic fields.

DOI: 10.1103/PhysRevLett.98.095002 PACS numbers: 52.50.Jm, 52.38.Fz, 52.70.La

Two MJ-scale laser facilities, the National Ignition Facility (NIF) [1] in the U.S. and the Laser Megajoule (LMJ) [2] in France, are being constructed to achieve ignition at the beginning of the next decade. The amount of energy available to drive the ablative implosion of an inertial confinement fusion (ICF) capsule, the stability and symmetry of the ablation front, mostly depend on the electron thermal conduction. The standard model for it is the Spitzer-Härm (SH) heat flux. Unfortunately, this theory fails at restituting actual observations and the SH flux must be artificially limited to some fraction f of the free-streaming flux; f is the first adjustable parameter in any hydrodynamic simulation of laser-plasma experiments. This points to an obviously nonpredictive character of ICF numerical codes.

The nonlocality of the heat carrying electrons [3–6] is often fingered as responsible for the heat flux inhibition. One-dimensional nonlocal or Fokker-Planck (FP) calculations usually give similar results as SH calculations with a 10% flux limitation. However 2D FP simulations [4] indicate that the lateral heat flux is much more inhibited than expected and the longitudinal heat wave is stronger. Another important 2D effect is the presence of self-generated magnetic fields [7–10]. The classical formulas by Braginskii [11] predict a reduction of the magnitude of the heat flux and its rotation through the Righi-Leduc effect. In the case of a single cylindrical laser beam aimed normally to a planar target, this rotation enhances the lateral conduction, opposite to the nonlocal effect. A combination of nonlocal and magnetic field effects have been investigated in small-scale simulations [12,13] but not yet checked in experiments nor incorporated in the large scale multidimensional radiation hydrocodes in spite of their importance for the ICF conditions.

We have developed recently new efficient algorithms [14] for modeling the electron transport issues in the ICF codes. They represent a significant effort to take a step beyond the flux-limited heat transport model, which has been a mainstay of the major, multidimensional ICF codes for more than a generation. This new model has been implemented in the 2D hydrodynamic code CHIC [15] for direct drive ICF modeling. The inclusion of both self-generated azimuthal magnetic fields and the non-Maxwellian electron distribution functions allows understanding of otherwise confounding transport in ICF targets. This Letter reports the results of an experiment specially designed to be highly sensitive to the dynamics of laser-produced heat waves under ICF conditions. We have used four beams of the LMJ prototype, the Ligne d'Intégration Laser facility (LIL) laser [16], which laser wavelength (0.35 μm), energy (multi-kJ) and pulse duration (several ns) are relevant to direct drive ICF. Its fundamental bandwidth, defined by a 14 GHz frequency phase modulation, is roughly 7 Å. Laser smoothing is achieved by combining longitudinal spectral dispersion and continuous-phase plates. The spectral dispersion is given by the 0.35-μm focusing gratings which produce quasi-Gaussian smooth 380 μm diameter focal spots with maximum intensity of 2×10^{15} W/cm^2. These features allow the observation of laser driven flows on long durations and with a good temporal resolution for the plasma parameters similar to future LMJ implosion experiments. The purpose of the experiment is to measure the velocity of the heat wave induced in a planar target for different laser intensities. During this campaign, seven successful shots were performed, with a laser energy varying from 4 to 10 kJ, pulse duration of 3 ns, corresponding to intensities from 8×10^{14} up to 2×10^{15} W/cm^2. At low intensities, we expect the

SH model to be correct. At high intensities, we surmise the appearance of long range electrons, responsible for nonlocal heating and self-generated magnetic fields at the hundreds kG level. To obtain the heat wave velocity, we observe the time dependent He-like emission of two thin metallic markers buried in a flat plastic disk (see Fig. 1). Marker layers embedded in planar or spherical targets [17] have already been used in order to characterize implosion performance or Rayleigh-Taylor (RT) growth by means of absorption spectroscopy [18,19]. In our case, the target disk is chosen thick enough, so that the rarefaction wave originating from the rear side of the target does not interact with the ablation front: the target is not accelerated and is therefore RT stable. The markers are V and Ti layers, buried either at 5 or 10 μm (V) and 15 or 30 μm (Ti) from the target surface: they produce He-like resonance lines at 5.2 keV and 4.7 keV, respectively. The 2D geometry related to the finite size of the focal spot launches naturally the competition between the nonlocal and magnetic field effects in the electron-energy transport. The markers thickness is constrained by two opposite trends: on the one hand, the markers should be thick enough to radiate a measurable signal on our detectors; on the other hand, the markers should be as thin as possible in order not to alter the heat flow. For this experiment, we used two series of thicknesses: 0.05 and 0.2 μm. The electron temperature and density in the V layer was inferred by high resolution emission spectroscopy. A curved Ge crystal spectrometer located at $\approx 12°$ to the laser direction was used to record the time-integrated V K-shell spectra. The emission lines, filtered by 10 μm Al plus 5 μm Cu foils, were recorded on Kodak DEF films. Intensity was deduced from the raw density data by using the Henke formula [20] and taking account of the filters and Ge crystal response [21]. At 10 kJ laser energy, the best fit of the space- and time-integrated spectrum with the code TRANSPEC [22] gives an average temperature of 2 keV for a mean density of 2.5×10^{21} cm^{-3} in the V layer. The ratio of the resonance to satellite lines is reasonably reproduced, as well as the ratio of H-like to He-like resonance lines. Observation of the time-resolved spectrum with our principal diagnostic, described below, shows that these parameters can be considered as average values during the laser pulse since the Heα line and its satellites are not noticeably changing during the emission time.

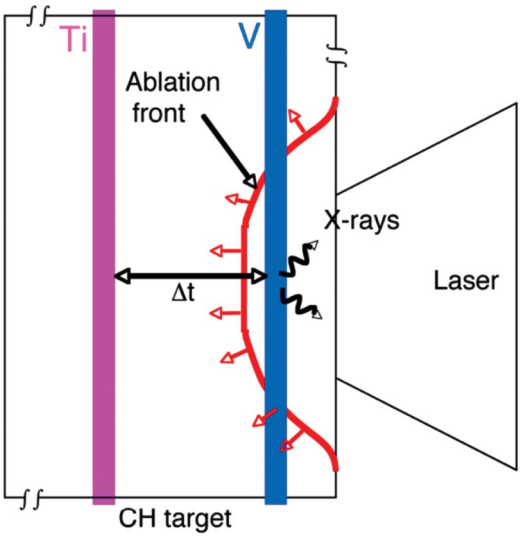

FIG. 1 (color). Principle of the experiment (not to scale). The heat flow velocity is measured from the time delay Δt of the X-ray emission of two buried layers of mid-Z materials.

The main diagnostic, located at 50° to the laser beam direction, is a cylindrically-bent highly oriented pyrolytic graphite (HOPG) crystal spectrometer [21]. Because of its high efficiency in the 4.5–5.5 keV spectral region of interest, we were able to couple it with a streak camera and detect a time-resolved spectrum of the V and Ti He-like emission lines, filtered by a 5 μm Cu foil, even for the thinnest 50 nm Ti and V layers. For each shot the time range was about 7 ns with a 100 ps resolution. Figure 2(a) shows raw experimental data at a laser energy of 7.2 kJ. This shot barely shows the Ti Lyα line in between lines labeled 1 and 2. However, the Heβ line is clearly visible, exhibiting a significant onset time delay with respect to the Heα line determined by the collisional excitation time of its upper level. In addition to Bragg crystal spectroscopy, DMX, a broadband absolutely calibrated time-resolved X-ray spectrometer [23] was used to cross-check the crystal measurements of the K-shell lines of the tracers; it also allowed us to follow the emission of the L shell (around 800 eV) and thus give a measurement of the heat wave foot velocity. The delay was determined from the time difference of the onset of the emission of both tracers above the bremsstrahlung background, the duration of which is consistent with the laser pulse duration. Results of the delay between the V and Ti emissions from both spectrographs are shown in Fig. 3 for several laser energies. Error bars include uncertainties on the onset times induced by the background noise and the detector response. There is an

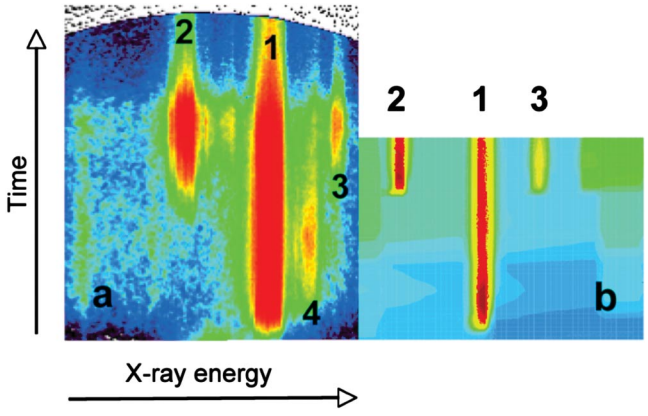

FIG. 2 (color). (a) Measured time-resolved spectrum, (b) CHIC simulation with flux-limited SH ($f = 0.07$). Laser energy is 7.2 kJ in both cases. 1: V Heα 5204 eV, 2: Ti Heα 4749 eV, 3: Ti Heβ 5581 eV, 4: V Lyα 5443 eV.

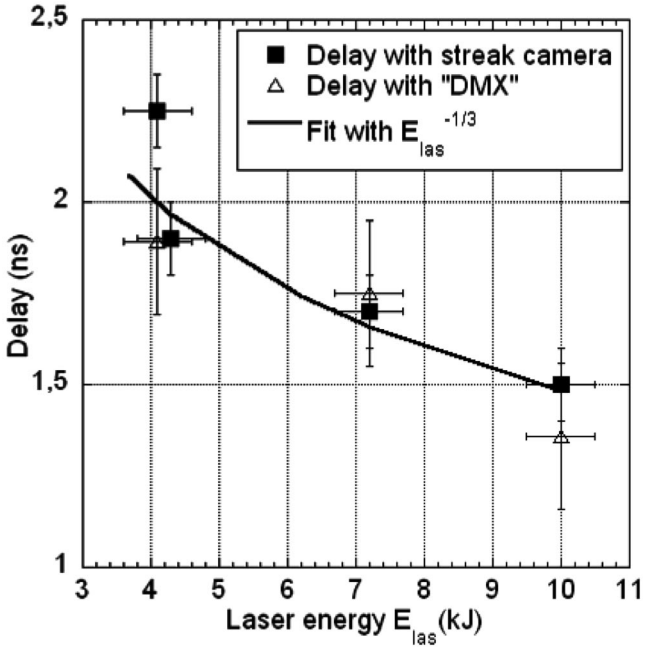

FIG. 3. Summary of results for the measured delays Δt between the onset of emission of 200 nm thickness V and Ti markers buried at 5 and 15 μm as a function of laser energy.

overall good agreement between the DMX and crystal data. The time delay varies with the inverse one third power of laser energy, i.e., the same scaling law as the inverse of the ablated mass rate.

We have used the 2D hydrodynamic code CHIC to simulate the laser-plasma interaction and the time-resolved tracer diagnostics [see Fig. 2(b)]. CHIC is a 2D, two-temperature code devoted to the design of direct drive ICF targets. The code solves the standard conservation equations for mass, momentum, and energy of the fluid in the Lagrangian formalism. The radiative transport is calculated assuming that the radiation field is quasistationary and weakly anisotropic (multigroup diffusion). The propagation and absorption of laser energy is calculated in the geometrical optics approximation with a 3D ray tracing package. CHIC uses the equations of state and ionizations in a tabular form. These tables are generated either by a Thomas-Fermi code or by a screened hydrogenic average atom model that provides radiation emissivities and opacities as well as ionization and electron pressures [24]. CHIC includes a flux-limited SH heat transport package and a new two-dimensional kinetic model for nonlocal transport including the effect of azimuthal magnetic fields [25]. Figure 2(b) shows the simulation of the time-resolved emission of the two markers under the laser and target conditions of Fig. 2(a). The agreement between experimental and computational data is gratifying although the measured time delay between He-α and He-β Ti emission is not correctly reproduced, presumably because of the crude atomic physics model used in the simulation (average atom model).

The nonlocal model rotates the heat flux with respect to the temperature gradient [4,5] because the lateral flux is more limited than the longitudinal component. The magnetic field reduces the conductivity along the gradient and generates a lateral flux (Righi-Leduc effect). Both nonlocal and magnetic fields effects reduce the heat flow in the direction of the temperature gradient, but they obviously compete in the lateral direction. The presence of magnetic fields thus mitigates the nonlocal effects on lateral transport, and may even cancel the delocalization of hot electrons [25]. The experimental data are very consistent with these theoretical predictions.

The complete set of performed calculations is summarized in Table I. The flux-limited SH model does not succeed at restituting the time-resolved measurements at the three energies with the same limiter. Nonlocal heat transport fails dramatically in the 7.2 kJ case and was not run at other energies. This is the clear indication of the magnetic field effects. Figure 4(a) displays lateral electron temperature profiles obtained at 1 ns after the onset of the laser pulse in CHIC calculations using either the SH, Braginskii, or the nonlocal model with magnetic fields included. One can observe that the nonlocal model produces a much warmer axial spot. This is related to a very strong inhibition of lateral heat transport. The temperature in the absorption region is about 3 keV and the heat is mainly carried by electrons with the energies of 8–10 keV. The mean free path of these electrons in the corona is close to 1 cm and their distribution is therefore nearly uniform in this region of the target, not producing any transverse heat flux any more. This effect has already been observed in 2D FP calculations [4]. Our simulations indicate that azimuthal magnetic fields of several hundreds of kG are generated on the edges of the focal spot. The corresponding Hall parameter $\omega_b\tau$ (the ratio of the electron gyrofrequency to the collision frequency) lies in the 0.1–0.5 range [see Fig. 4(b)]. A Hall parameter of 0.2 causes a 25% reduction of the heat flux magnitude, but also a rotation by 40° of its direction through the Righi-Leduc effect. In the geometry of the experiment, this rotation is clockwise, which enhances the lateral flux and slows the longitudinal heat wave. Nonlocal and magnetic field effects obviously compete as they predict opposite modifications of the lateral heat flux. Moreover, magnetic fields improve the validity of the

TABLE I. Comparison of theory and experiment for the emission delay (in ns) between the V and Ti markers.

Laser energy	4.2 kJ	7.2 kJ	10 kJ
HOPG crystal data	2.1 ± 0.1	1.75 ± 0.1	1.5 ± 0.1
Unlimited SH	1.9	1.45	1.0
Limited SH ($f = 0.07$)	2.45	1.75	1.5
Limited SH ($f = 0.1$)	2.05	1.65	1.35
Nonlocal	···	1.30	···
Braginskii	2.0	1.85	1.55
Nonlocal + B fields	2.15	1.75	1.5

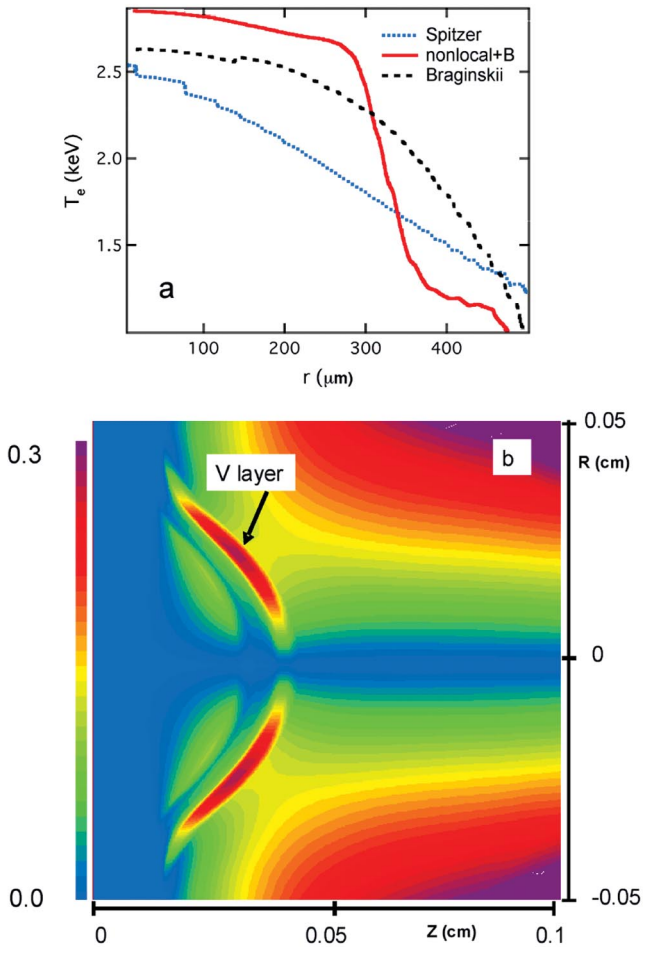

FIG. 4 (color). (a) Vertical lineouts (parallel to the target) of electron temperature at $t = 1$ ns, $z = 0.04$ cm for the three transport models. (7.2 kJ case). (b) Hall parameter distribution for the same time.

linear transport theory and moderate the nonlocal effects by reducing the effective range of high energy electrons to their gyroradius. In a plasma without magnetic fields this range scales as v^4, where v is the electron velocity, whereas the electron gyroradius is proportional to v. This analysis is confirmed by the results displayed in Table I: Braginskii calculation results fall within the experimental error bars at all energies, whereas inclusion of nonlocal effects in this model shows only minor improvements at 7.2 and 10 kJ. Finally, we observed that Braginskii calculations not including the Righi-Leduc effect (not shown) predict a much faster heat wave ($\Delta t \approx 1.55$ ns at 7 kJ), thus indicating that the rotation of the heat flux is an important feature of magnetized transport in ICF conditions.

In conclusion, our experiments proved to be sensitive to the modeling of the heat flow and to discriminate the heat inhibition effects. Analysis of the experimental data allows us to isolate the effects of heat flux modification both due to nonlocal effects and magnetic fields for the typical ICF conditions. The nonlocal heat transport alone is inadequate because it strongly inhibits lateral fluxes thereby producing a faster longitudinal heat wave than in the experiment. The dominant effect identified in our simulations is the presence of self-generated magnetic fields, which are shown to limit the range of high energy electrons, and to strongly affect the lateral transport through the Righi-Leduc term. Including these two effects in the CHIC code allowed us to reproduce the experimental results. Although the inclusion of nonlocal effects in the Braginskii model slightly improves the agreement between simulations and experiments, no clear evidence of nonlocal transport may be inferred from the experimental data. This confirms the leading role of magnetic fields on electron transport in direct drive ICF conditions.

This work was performed under the auspices of the Institut Lasers et Plasmas, which is in charge of the academic access to CEA laser facilities.

[1] E. I. Moses *et al.*, J. Phys. IV (France) **133**, 9 (2006).
[2] C. Cavailler *et al.*, Plasma Phys. Controlled Fusion **46**, B135 (2004).
[3] J.-F. Luciani *et al.*, Phys. Rev. Lett. **51**, 1664 (1983); J.-F. Luciani *et al.*, Phys. Rev. Lett. **55**, 2421 (1985); J.-F. Luciani and P. Mora, Laser Part. Beams **12**, 387 (1994).
[4] E. Epperlein *et al.*, Phys. Fluids B **3**, 3082 (1991); E. Epperlein *et al.*, Phys. Rev. Lett. **61**, 2453 (1988).
[5] G. Schurtz *et al.*, Phys. Plasmas **7**, 4238 (2000).
[6] A. V. Brantov *et al.*, Phys. Plasmas **5**, 2742 (1998).
[7] J. A. Stamper *et al.*, Phys. Rev. Lett. **26**, 1012 (1971).
[8] S. Glenzer *et al.*, Phys. Plasmas **6**, 2117 (1999).
[9] R. J. Kingham and A. R. Bell, Phys. Rev. Lett. **88**, 045004 (2002).
[10] T. K. Soboleva, S. L. Krasheninnikov, and P. J. Catto, Contrib. Plasma Phys. **44**, 95 (2004).
[11] S. I. Braginskii, in *Review of Plasma Physics*, edited by M. A. Leontovish (Consultants Bureau, New York, 1965), Vol. 1, pp. 205–311.
[12] T. H. Kho and M. G. Haines, Phys. Fluids **29**, 2665 (1986).
[13] A. V. Brantov *et al.*, Phys. Plasmas **10**, 4633 (2003).
[14] Ph. Nicolaï *et al.*, Phys. Plasmas **13**, 032701 (2006).
[15] J. Breil and P. H. Maire *et al.*, Report No. LRC-06.02, 2006; available at http://hal.inria.fr/inria-00113542
[16] J.-M. di Nicola *et al.*, J. Phys. IV (France) **133**, 595 (2006).
[17] D. K. Bradley *et al.*, Phys. Plasmas **5**, 1870 (1998).
[18] B. Yaakobi *et al.*, Phys. Plasmas **4**, 3021 (1997).
[19] T. R. Boehly *et al.*, Phys. Rev. Lett. **87**, 145003 (2001).
[20] B. L. Henke *et al.*, J. Opt. Soc. Am. B **3**, 1540 (1986).
[21] Ch. Reverdin *et al.*, Rev. Sci. Instrum. **75**, 3730 (2004).
[22] O. Peyrusse *et al.*, J. Phys. B **32**, 683 (1999); **33**, 4303 (2000).
[23] J.-L. Bourgade *et al.*, Rev. Sci. Instrum. **72**, 1173 (2001).
[24] S. Atzeni and J. Meyer-ter-Vehn, *Physics of Inertial Fusion* (Clarendon Press, Oxford, 2004).
[25] P. Nicolaï *et al.*, Phys. Plasmas **7**, 4250 (2000).